NUMERICAL AND EXPERIMENTAL INVESTIGATION OF POSTBUCKLING OF A COMPOSITE BOX STRUCTURE

M. Frey
Swiss Federal Aircraft Factory, Emmen, Switzerland
B. Graf, Dr.
Engineering Consultant, Zürich, Switzerland
S. Messmer, Dr.
Swiss Federal Institute of Technology, Zürich, Switzerland

Abstract

In this paper the postbuckling behaviour of a box like substructure of a carbon/epoxy-composite rudder for a fighter aircraft is studied by means of Finite Element Analysis (FEA). A series of experiments were conducted to verify the FEA-results, but also to address the stability, fatigue and strength of the structure. Investigation of dominant compression-, shear-, and combined buckling of skins of the structure revealed stable postbuckling behaviour. From nonlinear FEA reliable predictions for overall stiffness can be derived, whereas local quantities like membrane strains and curvatures of skins are sensitive with respect to modelling of boundary conditions and geometrical imperfections.

Introduction

Fibre-reinforced composite laminates are materials with high specific as well as absolute stiffness and strength and, therefore, are promising alternatives to conventional structural materials. Even though, widespread use of laminates has been mainly hindered because of lack of knowledge and experience with respect to material and structural behaviour as well as manufacturing techniques. Therefore these problems are subject of investigation in a "novel technology project" under way for the development of a carbon/epoxy-composite rudder for a fighter aircraft.

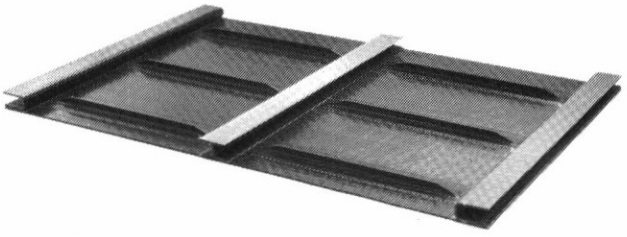

FIGURE 1- Structural Members of Specimen, Upper Skin Removed

Availability of reliable computational techniques for prediction of stiffness and stability would be a major contribution to improved quality assessment of preliminary design, as well as to savings by replacement or at least reduction of the number of tests required for qualification.

This paper covers the experimental verification of the predictive capabilities of such Finite Element Analysis (FEA). For these principal investigations a representative substructure of the rudder and three loading configurations are considered. The problem statement, experimental setup, FE-modelling as well as the presentation and discussion of results are outlined. Subsequently, some experimental results concerning aspects of fatigue and strength are also presented.

Problem Statement and Method of Approach

General

For the sake of simplicity, a representative box like substructure of the composite rudder has been considered. Structural members of this specimen are U- and I-shaped spars, upper and lower skins as well as stringers for stiffening of skins; cf. Figures 1 and 2. Skin sections bounded by spars and stringers are denoted as buckling fields.

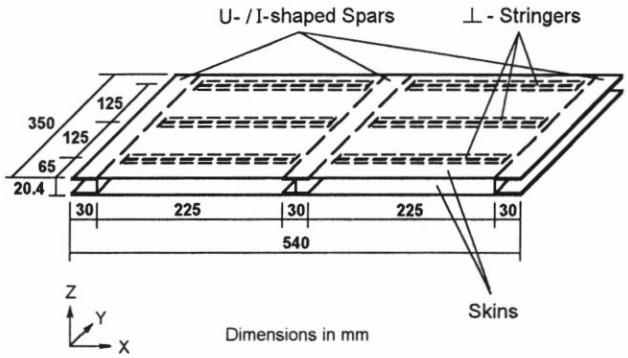

FIGURE 2 - Sketch with Dimensions of Test Structure

Copyright © 1994 by ICAS and AIAA. All rights reserved.

Loadcases

For the rudder as well as for the specimen the following main loadcases (LC) and corresponding dominant states of stress for the skins are distinguished :

- Bending (LCB). Induced by deflection of vertical tail, leading to compression or tension of skins.
- Torsion (LCT). Due to aerodynamic loading, leading to shear of skins.
- Combined (LCC). A combination of LCB and LCT, leads to combined tension/compression- and shear states of stress for the skins.

Stiffness and Stability of the Specimen

It can be assumed, that stiffness and stability is mainly influenced by the buckling of skins, because lateral buckling of spars is prevented. Considering a plate for modelling of skins, the problem statement for the specimen, therefore, will be outlined with the help of the well known problems, definitions, and results related to the buckling of plates (1).

Consider the simply supported elastic and rectangular plate depicted in Figure 3a. Loading under uniaxial compression (P) is assumed. In Figures 3b and 3c the predicted response is sketched in terms of midpoint deflection u_z and axial displacement u_x. First, the case of a perfect plate, i.e. with initial deflection $U_z = 0$ is discussed. Buckling is predicted for the Euler load P_E and is accompanied by a sudden onset of curvatures and deflections; whereas the latter is depicted in Figure 3b. Prior to buckling the problem is linear; cf. Figure 3c.

The following phenomena are related to the postbuckling regime, i.e. to loads $P > P_E$:

- Stiffness reduction, but overall stable behaviour; cf. Figure 3c.

- Redistribution of stresses; i.e. a larger portion of the load is taken by the portions of the plate near the lateral edges. The above mentioned drop of stiffness and stable postbuckling behaviour results from this redistribution. If the membrane strain for the centre of the plate is monitored, a linear increase with increasing compression is observed prior to buckling, followed by an underlinear increase in the postbuckling regime. Thus the onset of buckling and the buckling load can be identified with the help of this characteristic path of the membrane strain. Alternatively, also use could be made from the sudden onset of curvatures.

- Strong initial increase of deflections according to Figure 3b. Consequently the problem becomes geometrical nonlinear for large deflections $u_z/h > 1$ (h denotes plate thickness).

Owing to inevitable geometrical imperfections, i.e. $U_z \neq 0$, lateral buckling usually begins at a small load; cf. Figure 3b. For increasing geometrical imperfections, the problem type will change from the former stability problem to a geometrical nonlinear deformation problem. In the latter case, the Euler load is no longer significant for structural behaviour. For a further increase of imperfections the problem type might even change to that of a shell kind of stability problem. In either case, the problem is geometrical nonlinear.

For the specimen, also interaction of skins with spars and stringers have to be considered, leading to an even more complex response of the skins.

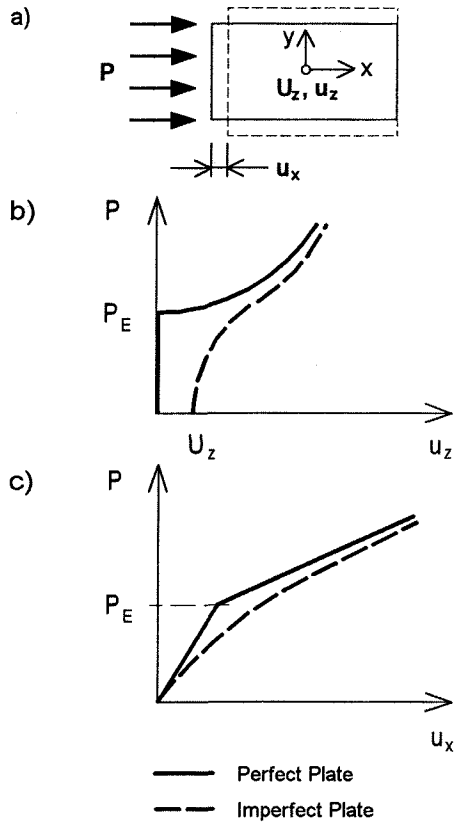

FIGURE 3 - Buckling of a Simply Supported Plate Under Compression :
a) Situation;
b) Load vs. Midpoint Deflection u_z, U_z : Initial Deflection;
c) Load vs. Axial Displacement u_x

However, using the insight gained from the previously discussed buckling of a plate, the problem statement for the specimen can now be designated more specifically :

- Numerical simulations with the help of linear and nonlinear FEA for prediction of :
  - Euler loads; i. e. critical loads related to the linear problem.
  - Buckling loads of skins. These loads will be defined with the help of the previously mentioned characteristics of membrane strains and/or curvatures. This definition makes use of the fact, that buckling is accompanied by the onset of significant stress redistributions, thus leading to pronounced changes of membrane strains and/or curvatures. For a perfect plate this approach is consistent with the definition of Euler loads and for imperfect plates seems to be an apparent and easy to apply definition of buckling. It also should be noted, that the application of Southwell plots (1), (2) relies on several restrictions and, therefore, is not suitable for the determination of buckling loads for the considered problem.
  - Significance of Euler loads for structural response. If the Euler loads and buckling loads of skins coincide, the critical loads of the specimen could be easily determined with the help of linear eigenvalue analysis.
  - Stiffness, i.e. load - displacement relationship in the pre- and postbuckling regime.
  - Stability in postbuckling regime, by means of inspection of load - displacement relationship and/or nonlinear buckling analysis.

- Verification of the predictive capabilities of FEA by comparison with experiments.

Experimental Investigations of Fatigue and Strength

Additionally, some aspects of fatigue and strength are investigated experimentally :

- Fatigue. Monitoring of stiffness and damage patterns (nondestructive ultrasonic C-scanning) for loading/unloading with 10 cycles up to design limit load, which for several reasons should coincide with the buckling load.

- Strength. Quasi static loading up to failure and inspection of the failure mechanism.

Experimental Setup

General

The specimen and loadcases are described in the previous section; cf. also Figures 1 and 2.

Stacking Sequence and Thickness of Structural Members

These data are listed in Table 1. Each layer is made up of a crossply carbon fabric and a toughened epoxy matrix.

Boundary Conditions and Loading

The setup allows for simulation of all of the loadcases by an easy adaptation of the positions of supports and loading points according to Figure 4; cf. also Figure 5 for a sketch of design of supports and loading points :

- LCB. Spars supported at one end and in the middle; loaded at the other end with point loads of equal magnitude.
- LCT. Spars supported at three corner points of the specimen; point load applied at the remaining corner.
- LCC. Spars supported like for LCB; two point loaded with fixed ratio of 2 to 1 applied at the ends of left U-shaped and I-shaped spar.

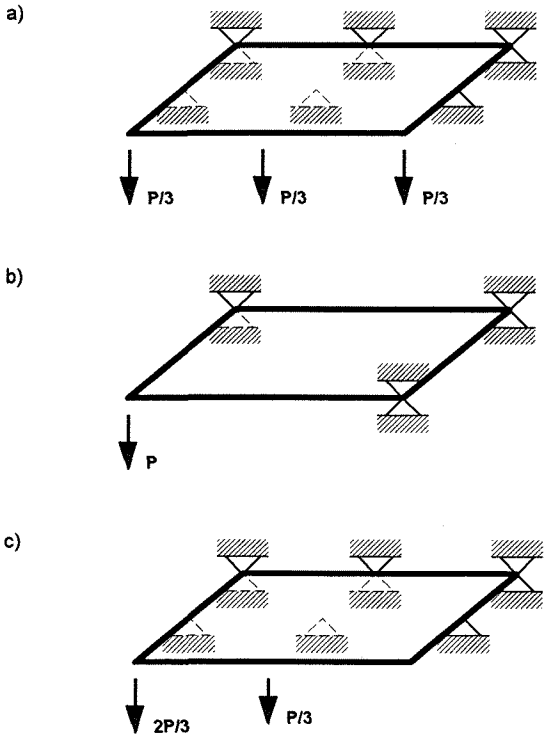

FIGURE 4 - Boundary and Loading Conditions: a) LCB, b) LCT, c) LCC

Structural Member		Stacking Sequence	Thickness [mm]
Skins		$[45/0/0/45/0/45_{1/2}]_s$	2.2
Spars	Flanges	$[0/45/0/45/0]_s$	2.0
	Web	$[0/45/0/45/0]_s$	2.0
Stringers	Flanges	$[0/45/0/0/45_{1/2}]_s$	1.8
	Web	$[0/45/0/0/45/0]_s$	2.4

TABLE 1 - Stacking Sequence and Thickness of Structural Members (Thickness According to Drawings)

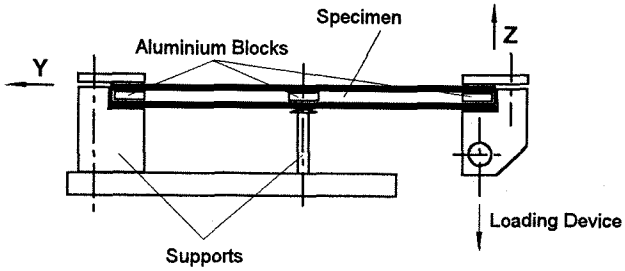

FIGURE 5 - Sketch of Design of Supports and Loading Devices (Side View of Specimen)

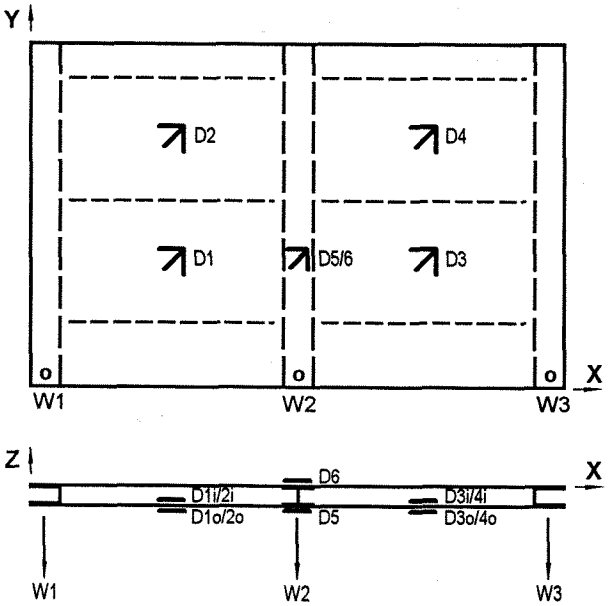

FIGURE 6 - Positions and Notations of Measuring Devices

The supports at the ends of the spars and the loading devices are similar in design, which allows for free rotations and shear, the latter in the plane of the webs of spars. The remaining bearings act as simple supports for the outer face of the lower skin. All the supports and loading devices are stiffened by aluminium blocks, clamped between the spar flanges. Thus, large deformations of flanges and webs due to concentrated forces are prevented.

Measuring Devices

The following quantities were measured at the positions indicated in Figure 6 :

- Deflections, at the loading points W1, W2, W3 for monitoring of global stiffness.
- Resultant of the forces applied at loading points.
- Normal- and Shear Strain Components. Strain gauge rosettes D1, D2, D3 and D4 were positioned at the centre of buckling fields. Strains were measured at inner and outer faces of the lower skin for evaluation of membrane strains and curvatures. Rosettes D5 and D6 were positioned in the symmetry plane of the specimen at the outer face of lower and upper skins.

Data Acquisition.

A data logger for switching of channels and a PC for monitoring and storage of data were used.

Test Procedure

- System Test. Loading within linear range at the beginning of each test for verification of plausibility and consistency of results.
- Buckling Test. Stepwise loading up to loads slightly above predicted Euler load.
- Fatigue Test. Repeated loading with 10 cycles up to buckling load. Examination of damage patterns prior and after test by ultrasonic C-scanning.
- Failure Test. Stepwise loading of specimen up to failure.

Finite Element Modelling

FE-Mesh

The FE-mesh of the specimen has a total of 18'000 degrees of freedom; cf. Figure 7 for subdivisions of lower skin. The discretisation and the choice of elements is based on benchmark solutions for the buckling of a rectangular plate under compression and shear (1). By subdivision of a buckling field into 4 x 8 quadrilateral thick shell elements, the FEA results match the theoretical Euler loads almost exactly. For the FE-model the geometric data according to drawings were used. Thus, the only imperfections of the skins are due to bending deflections of spars.

Boundary Conditions and Loading

Except for the simple supports, the bearings were modelled with the help of appropriate constraint conditions. Point loads were applied.

Material Behaviour

For modelling of composites the layer based material properties are required as input quantities. Orthotropic and linear elastic behaviour was assumed for the layers. With the elastic properties of fibres and matrix as well as the fibre content given, the orthotropic properties have been derived according to a proposal from Christensen (3). Comparison with experimental data, however, revealed large discrepancies. This could be traced back to unreliable matrix material data. Thus, experimental verification of the predicted orthotropic properties seems to advisable.

Only upper and lower bound solutions are known for prediction of the transverse shear modulus G_{23} (3), whereas for several reasons, usually no experimental data will be available for verification. It is common practice to set G_{23} equal to the inplane shear modulus G_{12}. This assumption is at least consistent with the upper and lower bound solutions mentioned above. For the specimen, transverse shear can be expected for the skins at the connections with the spars. Consequently, G_{23} is essential for the modelling of stiffness of skins. Thus, future experimental investigation of the transverse shear modulus seems to be desirable.

FE-Procedure for Geometrical Nonlinear Analysis

An Updated Lagrangian Approach (ULA) (4) and nonlinear buckling analysis, based on incremental stiffness matrices (5), were applied. Performance and convergence of the ULA were verified with the help of a benchmark solution. This is an approximate analytical solution for a simply supported imperfect plate, which holds up to moderate rotations. The MARC General Purpose Finite Element Code (5) was applied for FEA.

	Critical Loads [kN]		
	LCB	LCT	LCC
Euler Load (FEA)	9.3	1.7	4.7
Nonlinear FEA (*)	5.7	1.3	3.7
Experiment (*)	10.0	-	6.0

TABLE 2- Comparison of Critical Loads, (*) Buckling Loads of Skin

Review of Computational and Experimental Results

General

If not otherwise stated, both the computational and experimental data are plotted in the same figures. The positions of referenced measuring points are depicted in Figure 6. The results of the strain gauges D5 and D6 are not further outlined in this paper.

Euler Loads and Buckling Modes

The computational results for the buckling modes of the lower skin are shown in Figure 7 for all loadcases. The corresponding Euler loads are listed in Table 2.

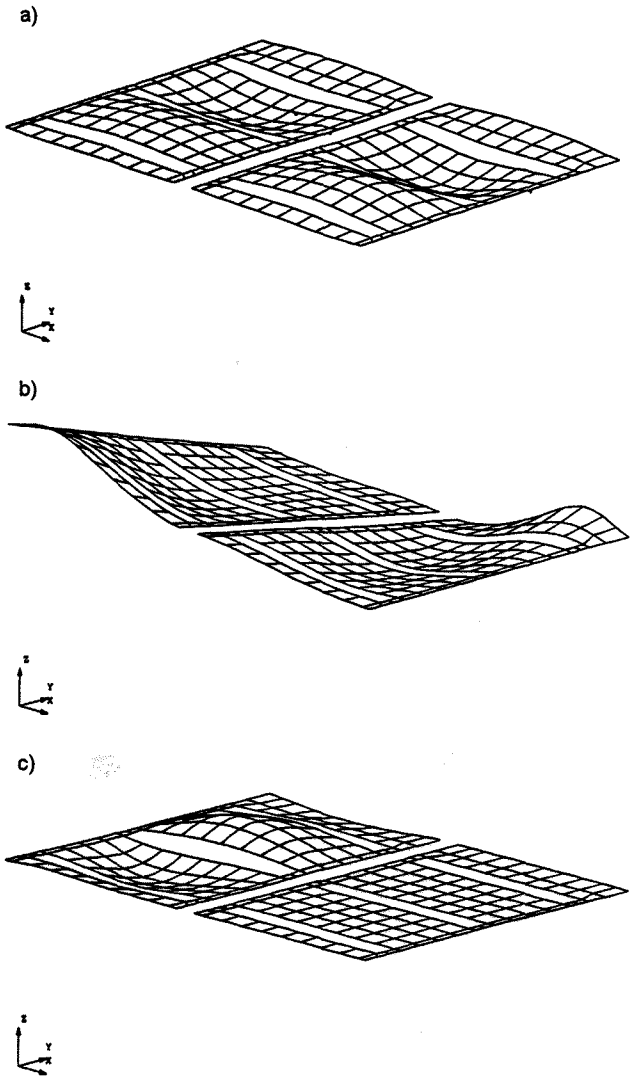

FIGURE 7 - Eigenmodes a for Lower Skin; Flanges of Spars and Stringers Removed : a) LCB, b) LCT, c) LCC

Deflections of Loading Points

The deflections of loading points W1, W2, W3 are plotted vs. the total applied loads for all loadcases in Figure 8. In experiment, only a load of 0.5kN, which is less than the Euler load, could be applied for LCT, due to very large deflections. For the remaining loadcases, the experimentally applied loads are greater than the Euler loads.

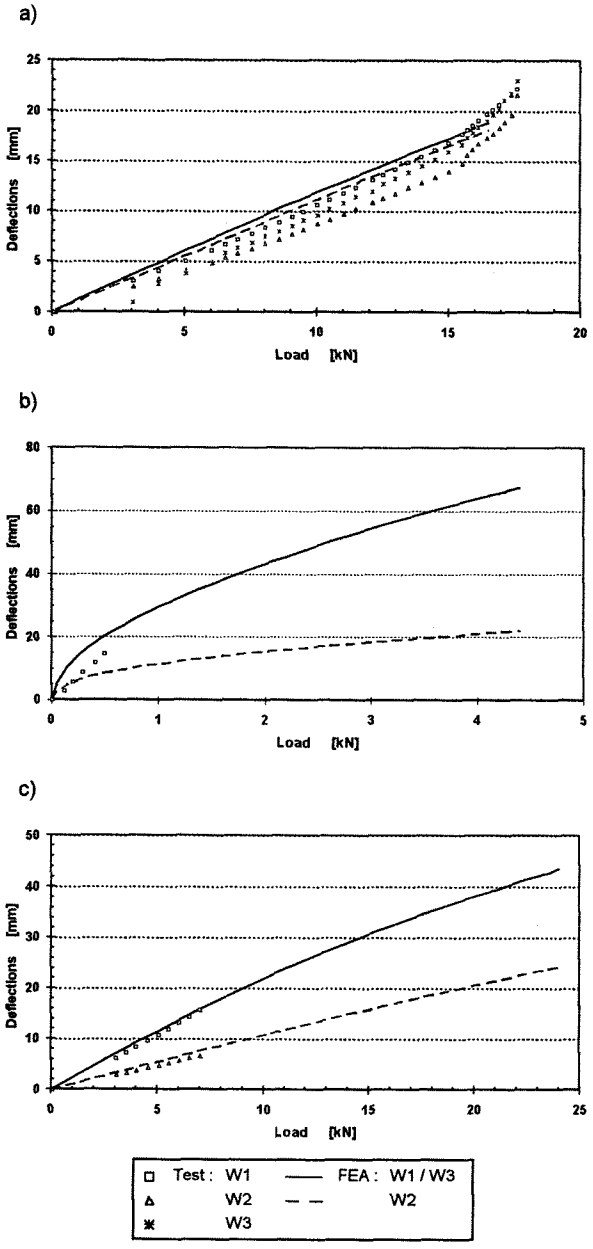

FIGURE 8- Deflections of Loading Points vs. Total Load : a) LCB, b) LCT, c) LCC

Membrane Strains and Curvatures at Centre of Buckling Fields

The membrane strains ε_x, ε_y, ε_{xy} and curvatures κ_x, κ_y, κ_{xy} are plotted vs. the total applied loads for all loadcases in Figure 9. The positions of monitored buckling fields can be identified with the help of the given notations for the related measuring devices; cf. title of Figure 9. The corresponding curvatures are plotted in an analogous way in Figure 10. No experimental data are available for loadcase LCT.

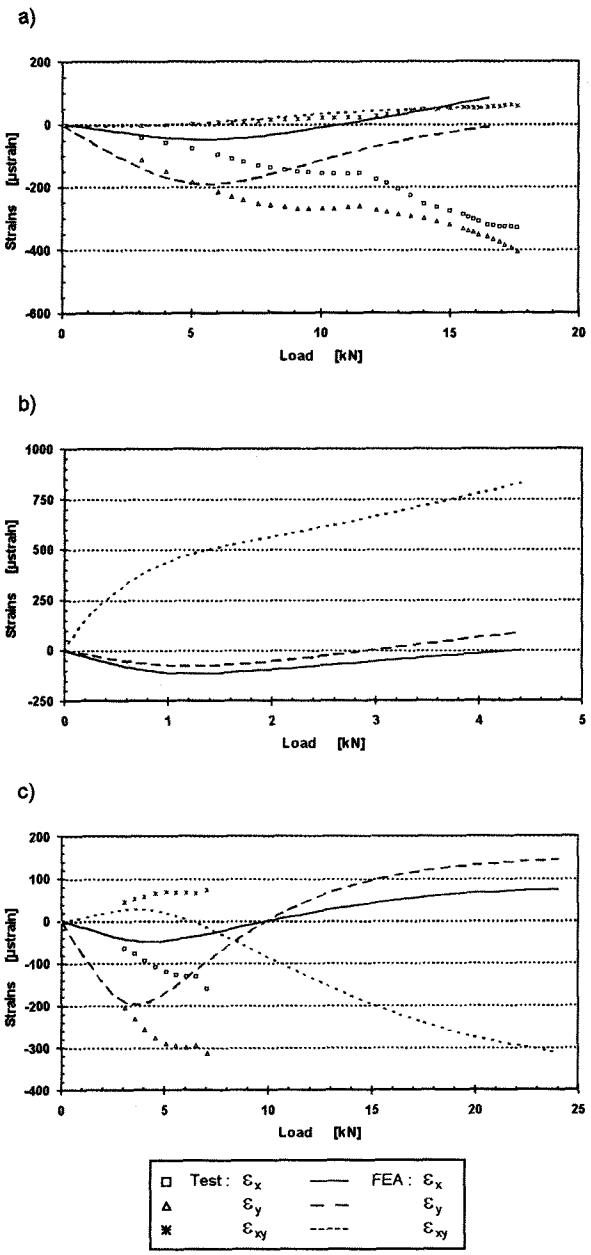

FIGURE 9 - Membrane Strains ε_x, ε_y, ε_{xy} at Centre of Buckling Fields vs. Total Load : a) LCB : Gauge D2, b) LCT : Gauge D4, c) LCC : Gauge D2

a)

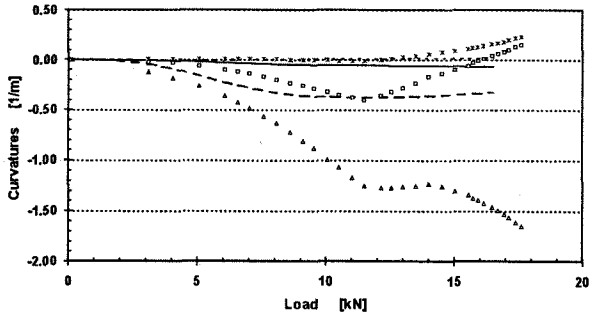

b)

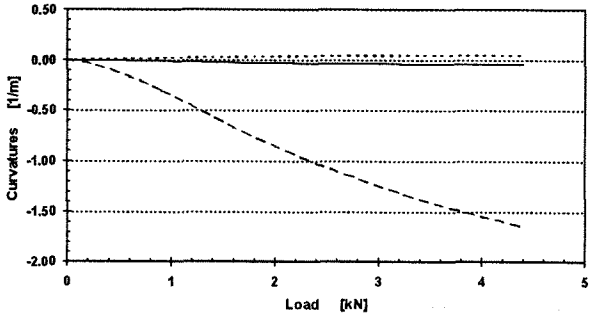

c)

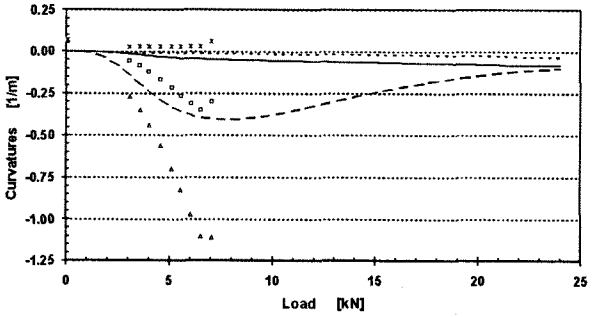

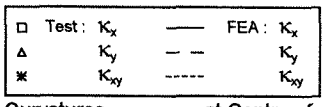

FIGURE 10 - Curvatures κ_x, κ_y, κ_{xy} at Centre of Buckling Fields vs. Total Load : a) LCB : Gauge D2, b) LCT : Gauge D4, c) LCC : Gauge D2

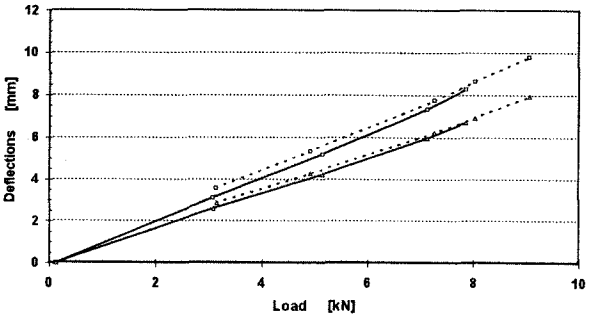

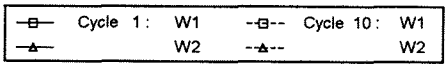

FIGURE 11 - Deflections of Loading Points vs. Total Load for Repeated Loading with LCB

Fatigue

Experimental data are available for LCB. The deflections of loading points are plotted vs. the total applied load in Figure 11. Further results will be outlined in context with the subsequent discussion.

Strength of Specimen

Experimental results are available for LCB and will also be further outlined in the subsequent section.

Interpretation, Comparison and Discussion of Results

Prediction of Stiffness and Stability from FEA

Euler Loads and Buckling Modes. According to Figure 7, the buckling patterns indicate good performance of the stringers. The eigenmodes of buckling fields are consistent with the ones to be expected from buckling of simply supported plates (1), if loaded under compression and/or shear. The Euler loads are listed in Table 2.

Buckling of Skins. The history of membrane strains ε_x and ε_y is characterised by an initially almost linear increase, followed by an extrema and subsequent decrease; cf. Figure 9. According to previously stated arguments, the buckling loads are defined as the loads, related to the extrema of membrane strains. These loads are listed in Table 2.

Continuos growth of curvatures indicate that lateral buckling begins at small loads as one would expect from the imperfections of skins, induced by bending deflections of spars, cf. Figure 10. Consequently, for the buckling loads no pronounced increase of curvatures is observed. It also should be noted, that the initial path of curvatures is strongly nonlinear.

Significance of Euler Loads for Structural Response. According to the critical loads from FEA listed in Table 2, buckling of skins and thus buckling of the specimen is overestimated by the Euler loads. This deviation is consistent with the observed nonlinear behaviour of curvatures prior to buckling; which contradicts the assumption of linear behaviour, related to Euler load estimates.

Stiffness in the Pre- and Postcritical Regime. Up to the buckling load, one would expect an almost linear behaviour and a subsequent drop of stiffness due to buckling. The latter holds true for LCB and loading point W3. For the remaining loading points and the same loadcase, as well as for all loading points and LCC, however, a small increase of stiffness is predicted, cf. Figures 8a,c. This increase might be caused by "geometrical hardening" due to the conservative loading, leading to an overcompensation of the drop of stiffness due to buckling. For the moderate deflections to be considered, this hardening effect is small. Consequently, the drop of stiffness is also small. For a simply supported plate under compression, the drop of stiffness is in the order of magnitude of 30%. For the considered loadcases LCB and LCC this drop is only a few percent. The latter might be affected by the boundaries of the buckling fields, which are perpendicular to the spars and are almost free. Due to the very large deflections related to loadcase LCT, this load-deflection relationship is strongly nonlinear; cf. Figure 8b.

Stability in the Postcritical Regime. According to Figure 8, the load-deflection curves indicate stable postbuckling behaviour for all loadcases. This has also been approved for LCC by nonlinear buckling analysis [5] and is in addition supported by the observation, that the buckling patterns do not change in shape. Consequently, collapse of the specimen can be expected from material failure.

Predictive Capabilities of FEA

Stiffness in Pre- and Postbuckling Regime. For the symmetric loadcase LCB, the measured deflections W1 and W3 differ up to 13%, whereas this value also gives the scatter of deflections from repeated tests. For both LCB and LCC, respectively, the deviations between predicted and measured deflections are less than 13%; cf. Figures 8a,c. Thus, the predicted stiffnesses are accurate.

Stability in the Postbuckling Regime. The results from FEA and experiments coincide; i.e. the buckling patterns do not change and a monotone increase of deflections is observed. Thus, both results indicate stable postbuckling behaviour.

Membrane Strains. A good qualitative coincidence is observed for the initially linear paths, derived from both experiment and FEA; cf. Figures 8a,c. For LCB steeper slopes are derived from FEA, exceeding the ones from experiment by factors of 1.5 and 1.1 for the ε_x and ε_y-strain components, respectively. The good coincidence of results for the y-direction is consistent with the previously discussed good coincidence of deflections of loading points.

The membrane strains for the y-direction is underestimated from FEA, which can be assumed to be mainly caused by the modelling of supports. As a consequence, buckling of skins is predicted for a lower critical ε_y-strain, than it is observed from experiments; cf. Figures 8a,c. This is consistent with the theoretical results for the critical membrane strains of simply supported plates under compression, which are by a factor of 1.4 larger for free lateral displacements if compared to the case of suppressed lateral displacements [5].

Also qualitative deviations are observed for the postbuckling regime; i.e. a decrease of membrane strains from FEA and increasing strains from experiments. This is likely due to the presumption, that collisions between stringers and skins occurred in experiments, whereas this contact problem has not been considered for FEA. Due to contact of both structural members a stabilising effect and thus increasing strains can be explained.

Buckling of Skins. The experimentally derived loads are listed in Table 2 for LCB and LCC. Comparison with the FEA-results reveals, that the skin buckling is underestimated by a factor of about 1.7, which is consistent with the previous discussion of membrane strains. The buckling patterns are consistent with the predictions.

Curvatures. Both greater qualitative and quantitative deviations are observed between calculated and measured results, than for the above mentioned membrane strains; cf. Figures 10a,c. This is mainly due to the well known pronounced sensitivity of curvatures with respect to initial curvatures of skins, which have not been considered for FEA. Basically, the computational results could be approved by considering measured imperfections of the specimen. On the other hand, such data are usually not available for design. Consequently, predicted bending stresses will inherently be more inaccurate than predictions of stiffness and membrane strains.

Fatigue

Inspection of the deflection history indicates no stiffness changes due to repeated loading; cf. Figure 11. This is also consistent with the results of ultrasonic C-scanning, which revealed no damages.

Failure Test

Stepwise loading was applied up to collapse of the specimen for LCB; cf. Figure 8a. At a load level of 14 kN, the onset of progressive failure of fibres was indicated by noises. The onset of decreasing stiffness was first observed from the load-deflection curve for the I-shaped spar at a load level of 15.5 kN. Collapse occurred at a load of 18kN, which is almost twice the experimentally found buckling load. For this load shear failure was observed for the web of one of the U-shaped spars.

Summary and Conclusions

Buckling of the specimen is governed by buckling of skins. Due to geometrical nonlinear behaviour prior to buckling, Euler load estimates are not suitable for prediction of buckling loads. From the results of nonlinear FEA, the buckling load can be identified from the characteristics of the shape of curve of the membrane strains for the centre of a buckling field. Such characteristics are the maximum membrane strain or the onset of a constant path, following the almost linear behaviour for the *prebuckling regime*.

For both loadcases LCB and LCC almost linear load-displacement relationships are predicted for the pre- and postbuckling regimes. This almost linear behaviour indicates also a small drop of stiffness due to buckling, which is compensated or overcompensated by hardening effects due to conservative loading. It also should be noted, that this small drop of stiffness might be a result of the partially almost free boundaries of buckling fields of the specimen. Thus, for buckling in the centre of a large skin field of the rudder, one would expect a larger drop of stiffness. Due to very large deflections, the stiffness behaviour is strongly nonlinear for loadcase LCT. In either case, however, the postbuckling behaviour is stable. This is also supported by the observed buckling patterns of skins, which do not change in the postbuckling regime.

The deviations between measured and calculated deflections of loading points are less than 13%, whereas the latter value reflects the scatter to be expected from repeated experiments.

Observed deviations of membrane strain histories are likely due to an overestimation of lateral stiffness in FEA and contact of stringers and skins for large deformations, whereas latter has not been considered for FEA. As a consequence of the overestimated lateral stiffness, buckling of skin is predicted for smaller critical membrane strains than observed from experiments. Due to the stabilising contact effect, increasing membrane strains are observed in the postbuckling regime in the tests, whereas a decrease is predicted. Basically, these discrepancies between predictions and experiments could be resolved by modelling refinements like adaptation of stiffness of supports and o the transverse shear modulus, to adjust the lateral stiffness, as well as by considering the contact problem.

Large discrepancies for predicted and measured curvatures are related to the highly imperfection sensitivity of this quantity. Thus, such discrepancies seem to be unavoidable and consequently have to be covered by appropriate careful interpretation of the predicted bending stresses.

No fatigue was observed for loadcase LCB under repeated loading up to buckling load, from monitoring of stiffness and damage patterns. For LCB the specimen collapsed under almost twice the buckling load due to shear failure of the web of one of the U-shaped spars, which is also an additional *proof of stable postbuckling behaviour*.

Thus, accurate FEA-predictions of the stability of a complex box-like composite structure are feasible, even in the draft state of design as usually the required input data are available. Consequently, design costs can be reduced by at least partial replacement of prototype testing by FE-simulations.

Acknowledgement

This paper is the result of a research and development project partially supported by the Swiss Defence Technology and Procurement Agency.

References

(1) Timoshenko, S.P.; Theory of Elastic Stability, McGraw Hill, New York, 1926
(2) Bushnell, D.; Computerized Buckling Analysis of Shells, Martinus Nijhoff Publishers, 1985
(3) Christensen, R.M.; Mechanics of Composite Materials, John Wiley & Sons Inc., New York, 1979
(4) Bathe, K.J.; Finite Element Procedures in Engineering Analysis, Prentice Hall Inc., 1982
(5) MARC User Information Manual, Rev. K4, MARC Analysis Research Corporation, Palo Alto CA